Electronic Supplementary Material (ESI) for Environmental Science: Nano.
This journal is © The Royal Society of Chemistry 2024

Supporting Information

Deep eutectic solvent-assisted dual valorization of waste distillers' grains-derived lignocellulose: pyrolyzed hydrochar microflowers-supported peroxymonosulfate activation and lignin carbon dots-aided Fe^{3+} detection

Cheng Huang [a, b], Yunbo Zhai [a, b, *], Xiangmin Liu [c], Xiaoping Liu [d], Zhexian Wang [a, b], Yin Zhou [a, b], Hanzhuo Luo [a, b], Deyu Qin [a, b], Chen Zhang [a, b, *]

[a] *College of Environmental Science and Engineering, Hunan University, Changsha 410082, P.R. China*

[b] *Key Laboratory of Environmental Biology and Pollution Control (Hunan University), Ministry of Education, Changsha, 410082, P.R. China*

[c] *Institute of Microbiology, Jiangxi Academy of Sciences, Nanchang 330012, China*

[d] *School of Land Resources and Environment, Jiangxi Agricultural University, Nanchang 330045, P.R. China*

[*] Corresponding author.

E-mail addresses: ybzhai@hnu.edu.cn (Y. B. Zhai), zhangchen@hnu.edu.cn (C. Zhang)

1. Materials and methods

Materials

Distillers' grains were obtained from Gujing Group in Bozhou, Anhui Province, China. The distillers' grains were washed with plenty of water to remove impurities, leaving a clean rice husk, which is often used as a filler for solid-state fermentation. Rice husks were thoroughly dried at 60 °C and then crushed. Pass through a 60-mesh sieve and set aside. All chemical reagents used in the experiment are analytically pure without further purification.

DESs preparation and pretreatment of distillers' grains

The $AlCl_3 \cdot 6H_2O$: Glycerol (1:8 mol/mol) DESs were synthesized by heating and stirring in an oil bath at 80 °C. The mixtures were continuously stirred until a uniform, transparent liquid was formed (Fig. S1). In the formed DESs, glycerol is the hydrogen bond donor and $AlCl_3 \cdot 6H_2O$ is the hydrogen bond acceptor. Then, $AlCl_3 \cdot 6H_2O$: Glycerol (1:8 mol/mol) DESs were used to pretreat the dry distillers' grains powder, the specific steps were as follows: about 1g of powder was mixed with 15 parts DESs in a clear high-borosilicate glass bottle, heated and stirred at 80, 90, 100, 110, 120, 130 °C for 4 h to explore the optimal pretreatment temperature. In addition, in order to explore the effect of time on the deconstruction of lignocellulose, pretreatment time were set at 110 °C for 1, 3, 5, 7, 9 h.

Conversion of cellulosic carbohydrates into PHMs

The pre-treated product was poured into a mixture of acetone/water (7:3 v/v) and stirred vigorously at room temperature for 3 h. A high-speed centrifuge was used to separate the pretreated biomass solid fraction (SF) and the liquid fraction (LF) at 10000 rpm for 3 min. The solid cellulose residue

was obtained by washing SF three times with 70% acetone aqueous solution. After centrifugation, the LF was evaporated by rotation at 50 °C to remove acetone to obtain a concentrated suspension containing DES-extracted lignin as a precursor of carbon dots.

Synthesis of hydrochar microspheres (HMs): the solid cellulose residue was dried in a freeze-drying oven to completely remove the water. Then, 0.6 g solid was added to 15 mL water (40 $g \cdot L^{-1}$), stirred for 4 h, and reacted at 220 °C for 4 h in a 50 mL Teflon-lined stainless-steel autoclave. The product after the hydrothermal reaction was dried at 60 °C overnight in a vacuum drying oven.

Synthesis of PHMs: Take 0.4 g of obtained HMs, 1.2 g of cobalt acetate, 2.4 g of $KHCO_3$, and 0.2 g of melamine and grind them together in an agate mortar to achieve uniform blending. The resulting mixture was then transferred to a corundum ship and annealed in a tube furnace at 800 °C for 1 h. After grinding, the PHMs was obtained by washing with 1 M hydrochloric acid and ultra-pure water.

Synthesis of carbon dots from separated lignin

The LCDs were prepared by solvothermal method. In brief, the concentrated suspension containing DES-extracted lignin was collected, and 54 mL was taken into a 100 mL Teflon-lined stainless-steel autoclave and heated at 180 °C for 6 h. The obtained yellow solution was centrifuged at 10000 rpm for 10min to separate the liquid phase portion containing carbon dots. Then, the LCDs aqueous solution was obtained by filtration through a 0.22 μm filter and dialysis for 48 h in a dialysis bag with a molecular weight cutoff of 1000 Da.

Antibiotics degradation experiments

The peroxymonosulfate (PMS) activation performance of PHMs were evaluated in a 150 mL conical flask containing 100 mL of reaction solution. In a typical experiment, a certain amount of

PHMs activator is uniformly dispersed into 100 mL of solution containing antibiotic contaminants at room temperature. Then, 1 mL 100 mM PMS solution is quickly injected into the contaminant solution to initiate the reaction. At a set time point within 10 min, 1 mL of the mixed reaction solution was sampled and passed through the 0.22 μm PTFE filter to remove the PHMs activator. The concentration of contaminants was measured by high performance liquid chromatography (HPLC, Agilent, 1260 Infinity II, USA) to obtain the reaction curve. The corresponding parameter settings and mobile phase selection of different pollutants are shown in the HPLC operation. Then, the kinetic rate constants (k_{obs}) of pollutant removal could be calculated by the following kinetic equations:

$$\ln\frac{C_t}{C_0} = -k_{obs} \times t \#(1)$$

where $[C]_0$ *and* $[C]_t$ are the concentrations of pollutants at the beginning of reaction and reaction time (t), respectively.

Moreover, to evaluate the viability for practical applications, the continuous-flow degradation of tetracycline (TC) was carried out using a reactor consisting of a microfiltration membrane supported by a nylon substrate, filled with PHMs activator. Firstly, 50 mg PHMs was added to 300 mL ultra-pure water and ultrasonic for half an hour to obtain the dispersed PHMs suspension. Then, the PHMs suspension was directly vacuumized to deposit the PHMs on the nylon substrate, and the PHMs/Nylon composite microfiltration membrane was constructed.

Fluorescent detection of Fe^{3+}

The detection of heavy metal ions (Mg^{2+}, Zn^{2+}, Co^{2+}, Ca^{2+}, Ba^{2+}, Ni^{2+}, Cr^{3+}, Pb^{2+}, Cu^{2+}, Fe^{3+}) by LCDs were performed at room temperature in aqueous solution. In a typical run, 2 mL LCDs solution was added into 3 mL heavy metal ions solutions with concentration of 500 μM. In order to

prove the sensitivity of LCDs to Fe^{3+}, different concentrations of Fe^{3+} were added to the solution containing the same number of LCDs, and the fluorescence spectrum of the mixed solution were recorded at the excitation wavelength of 360 nm after 10 min of equilibrium. F_0 represents the fluorescence intensity of the control group without metal ions, F represents the fluorescence intensity of LCDs quenched by metal ions, and $(F_0\text{-}F)/F_0$ represents the relative fluorescence intensity. The standard curve was established by linear fitting of the relative fluorescence intensity ($(F_0\text{-}F)/F_0$) and the metal ions concentration.

HPLC operation

TC: The concentration of TC was determined by HPLC (Agilent 1260 Infinity II, USA) with an Agilent EC-C18 column (4.6 × 250 mm, 5 μm). The mobile phase was a mixture of 80% acetonitrile and 20% water with oxalic acid (10 mmol/L). The flow rate and injection volumes were 1 mL/ min and 20 μL, respectively. The detector wavelength was set at 270 nm.

SMZ: The concentration of SMZ was determined by HPLC (Agilent 1260 Infinity II, USA) with an Agilent EC-C18 column (4.6 × 250 mm, 5 μm). The mobile phase was a mixture of 35% acetonitrile and 65% water. The flow rate, injection volume, and detection wavelength were set at 1 mL/min, 20 μL, and 266 nm, respectively.

SMX: The concentration of SMX was determined by HPLC (Agilent 1260 Infinity II, USA) with an Agilent EC-C18 column (4.6 × 250 mm, 5 μm). The mobile phase was a mixture of 35% acetonitrile and 65% water. The flow rate, injection volume, and detection wavelength were set at 1 mL/min, 20 μL, and 266 nm, respectively.

CIP: The concentration of CIP was determined by HPLC (Agilent 1260 Infinity II, USA) with an Agilent EC-C18 column (4.6 × 250 mm, 5 μm). The mobile phase was a mixture of 20% acetonitrile and 80% water with 0.1% formic acid. The flow rate and injection volumes were 1 mL/

min and 20 μL, respectively. The detector wavelength was set at 272 nm.

ENR: The concentration of ENR was determined by HPLC (Agilent 1260 Infinity II, USA) with an Agilent EC-C18 column (4.6 × 250 mm, 5 μm). The mobile phase was a mixture of 30% methanol and 70% water with 0.2% formic acid. The flow rate and injection volume were 1 mL/min and 20 μL, respectively. The detector wavelength was set at 293 nm.

Characterization methods

Scanning electron microscope (SEM, Zeiss Sigma 300) coupled with an energy disperse X-ray spectroscopy (EDS, FEI Tecnai F20) was employed to acquire the morphologies and elemental distribution of the samples. The X-ray diffraction (XRD, Bruker D8 Advance instrument) was tested with Cu Kα radiation from 80° to 10°. Raman spectra was recorded to track changes in the defective and graphitic structures of PHMs (λ = 514 nm). The X-ray photoelectron spectroscopy (XPS, Thermo Scientific K-Alpha spectrometer) was tested to detect the quantity and state of surface elements. Electron paramagnetic resonance (EPR, Bruker A300 spectrometer) signals were recorded to measure the generation of reactive species with 5,5-dimethyl-1-pyrrolidine N-oxide (DMPO) as spin-trapping agent. Linear sweep voltammetry (LSV, Chenhua CHI 760E electrochemical workstation) was investigated with a three-electrode cell, details of the method was shown in Linear Sweep Voltammetry Test. The UV absorption spectrum of the LCDs sample was tested using an UV-Vis spectrometer model E500 with a scanning range of 200-500 nm. The fluorescence excitation and emission spectra of the LCDs samples were measured by the Japanese F-4600 fluorescence spectrophotometer.

Linear Sweep Voltammetry Test

Linear sweep voltammetry was measured on an electrochemical station using a three-electrode system. The glassy carbon electrode was used as the working electrode, and the Pt electrode and Hg/Hg_2Cl_2 electrode were used as the counter electrode and the reference electrode, respectively. Phosphate buffer (pH ~7, 20 mM) was used as the electrolyte for the LSV test. During the test, a certain amount of PMS or TC was added into the electrolyte to investigate the electron transfer process between PHMs and PMS or TC. The voltage was increased from 0 to 1.6 V at a scanning rate of 20 mV/s.

2. Figures and Tables

Fig. S1 Flow chart for synthesis of $AlCl_3 \cdot 6H_2O$: Glycerol (1:8 mol/mol) DESs.

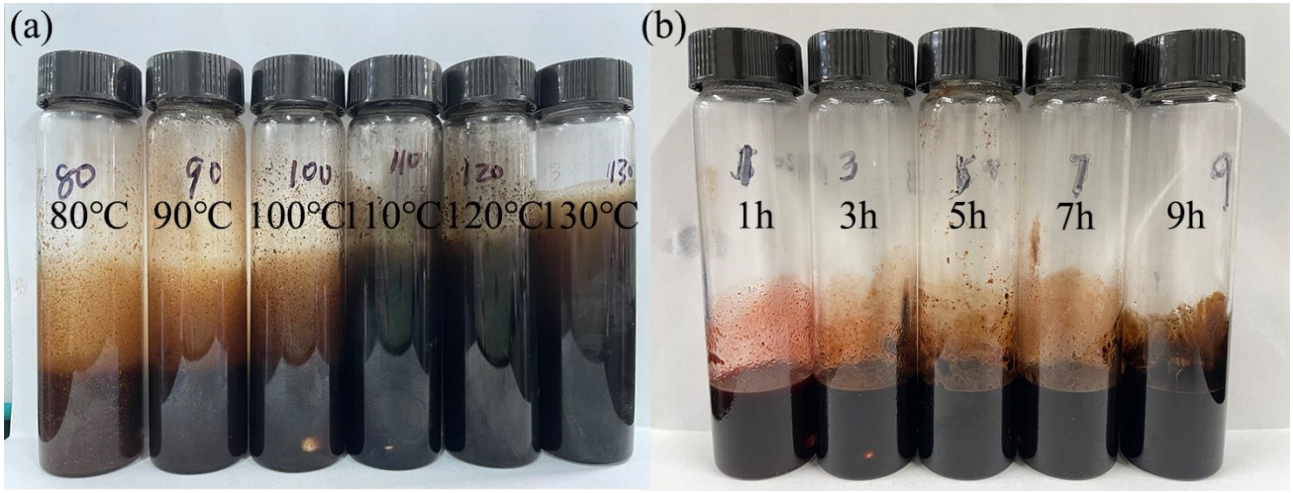

Fig. S2 DESs pretreatment of lignocellulose from distillers' grains (a) under different temperatures condition for 4 h, (b) under different time at 110 ℃.

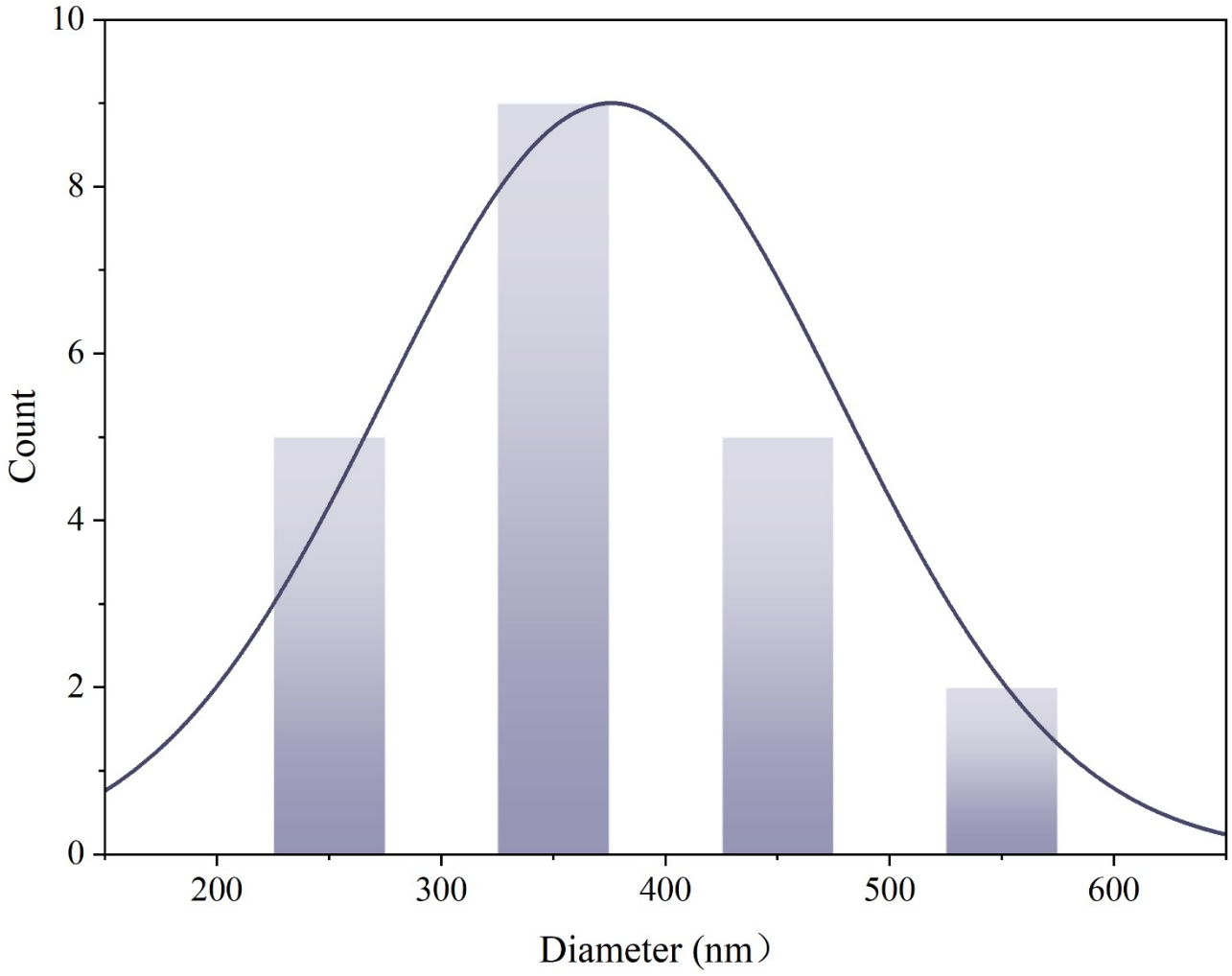

Fig. S3 Particle size distribution of PHMs.

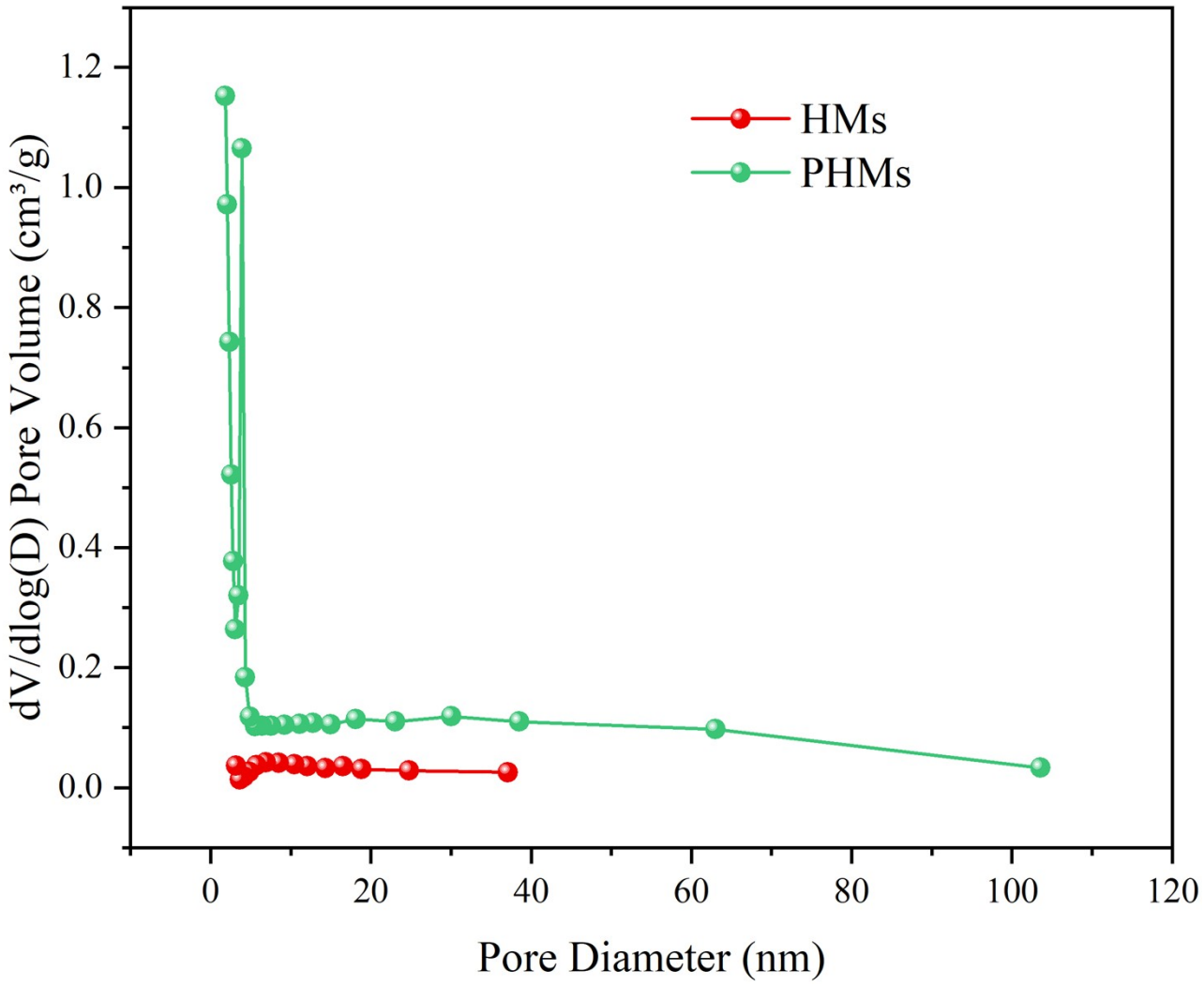

Fig. S4 Pore size distribution of HMs and PHMs.

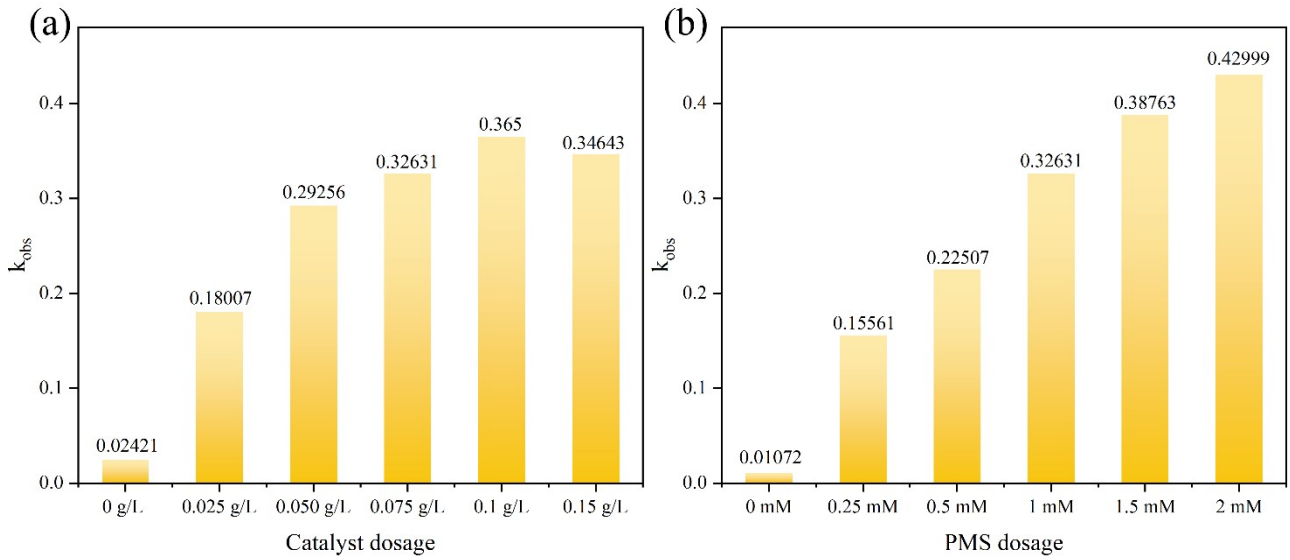

Fig. S5 k_{obs} of different conditions: (a) catalyst dosage, (b) PMS dosage.

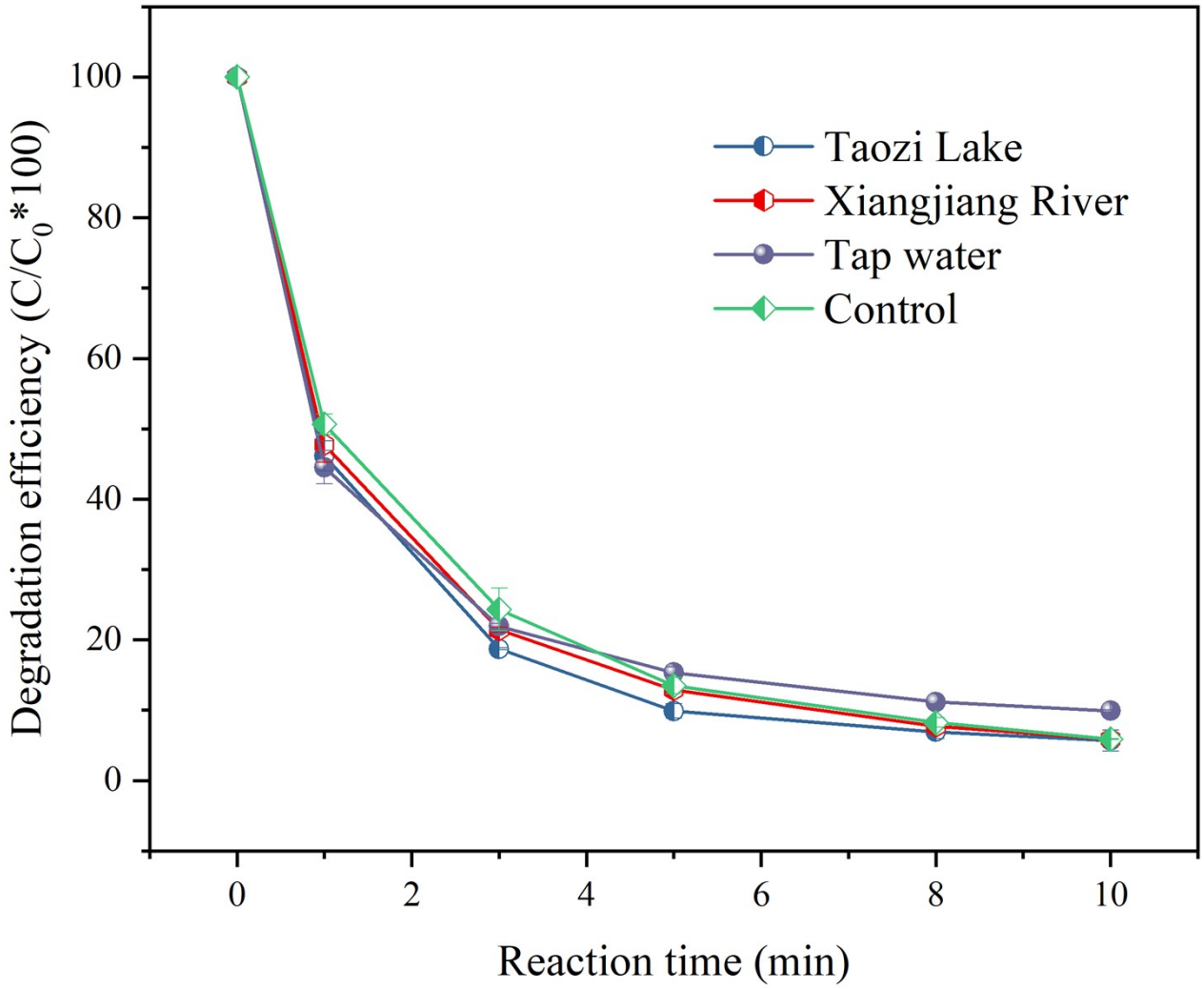

Fig. S6 Effect of different water samples condition on TC degradation. Reaction conditions: $[TC]_0$ = 30 mg·L^{-1}, [PMS] = 1 mM, catalysts = 0.075 g·L^{-1}, T = 25 °C, initial pH = 6.5.

Table. S1 Comparison with other biochar catalysts derived from biomass in literature.

Biochar catalyst derived from biomass	Dosage	PMS	Pollution	k (min^{-1})	k/ Dosage ($L\ min^{-1}\ g^{-1}$)	Reference
Distillers' grains	0.075 g/L	1 mM	Tetracycline	0.3263	4.35	This study
Poplar and pine sawdust	3.0 g/L	3 mM	Tetracycline, Chlortetracycline, Doxycycline	0.0588	0.02	[1]
Walnut shell	3.0 g/L	5 mM	Norfloxacin	0.0292	0.01	[2]
Passion fruit shell	0.4 g/L	0.3 g/L	Tetracycline	0.0317	0.08	[3
Digestate	1.0 g/L	2.50 mM	Sulfanilamide	0.0245	0.02	[4]
Sludge	2.0 g/L	0.6 mM	Ciprofloxacin	0.0140	0.01	[5]
Pinewood	0.2 g/L	3 mg/L	Ciprofloxacin	0.0530	0.27	[6]
Moso bamboo	3.0 g/L	5 mM	Tetracycline	0.0915	0.03	[7]
Banyan branch	0.75 g/L	2 mM	Metronidazole	0.0566	0.08	[8]
Sludge	0.75 g/L	0.75 g/L	Doxycycline	0.2493	0.33	[9]
Cow manure	0.05 g/L	0.4 mM	Carbamazepine	0.2020	4.04	[10]
Sheep manure	0.6 g/L	0.6 g/L	Sulfadiazine	0.0680	0.11	[11]
Piggery sludge	0.02 g/L	0.5 mM	Tetracycline	0.0107	0.54	[12]
Straw	0.4 g/L	0.4 mM	Ciprofloxacin	0.0566	0.14	[13]
Pig carcass	0.8 g/L	0.5 mM	Sulfamethoxazole	0.0409	0.05	[14]
Gingko leaf	0.1 g/L	7 mM	Sulfamethoxazole	0.1397	1.40	[15]
Durian peel	0.3 g/L	0.5 g/L	Ofloxacin	0.0160	0.05	[16]
Hyperaccumulator residues	0.2 g/L	1 mM	Bisphenol-A	0.158	0.79	[17]
Tea leaf powder	0.1 g/L	0.3 g/L	Tetracycline	0.26	2.60	[18]
Bamboo leaf	0.2 g/L	0.2 g/L	Bisphenol-A	0.1410	0.705	[19]
Enteromorpha powders	0.2 g/L	0.5 mM	Sulfadiazine	0.0764	0.38	[20]
Chitosan	0.05 g/L	2 mM	Bisphenol-A	0.0270	0.54	[21]
Fresh swine manure	0.4 g/L	1 mM	Sulfamethoxazole	0.0376	0.09	[22]

Table. S2 Comparison of different fluorescent nanoprobes for Fe^{3+} detection in the literature.

Fluorescent nanoprobes	Linear range (μM)	Reference
Carbon dots	12.5-100	[23]
Lignin carbon dots	10-50	[24]
Nano-biomass dots	0-30	[25]
Nitrogen doped carbon dots	0-50	[26]
Graphene carbon dots	0-80	[27]
Nitrogen and sulfur doped fluorescent carbon dots	0.25-125	[28]
Lignin-derived carbon dots	10-150	This work

3. Supplementary References

1. Y. Zhang, M. Xu, S. Liang, Z. Feng and J. Zhao, Mechanism of persulfate activation by biochar for the catalytic degradation of antibiotics: Synergistic effects of environmentally persistent free radicals and the defective structure of biochar, *Sci. Total Environ.*, 2021, **794**, 148707.
2. Y. Zhang, M. Xu, X. Liu, M. Wang, J. Zhao, S. Li and M. Yin, Regulation of biochar mediated catalytic degradation of quinolone antibiotics: Important role of environmentally persistent free radicals, *Bioresour. Technol.*, 2021, **326**, 124780.
3. Y. Hu, D. Chen, R. Zhang, Y. Ding, Z. Ren, M. Fu, X. Cao and G. Zeng, Singlet oxygen-dominated activation of peroxymonosulfate by passion fruit shell derived biochar for catalytic degradation of tetracycline through a non-radical oxidation pathway, *J. Hazard. Mater.*, 2021, **419**, 126495.
4. Y. Wang, Y. Song, N. Li, W. Liu, B. Yan, Y. Yu, L. Liang, G. Chen, L. a. Hou and S. Wang, Tunable active sites on biogas digestate derived biochar for sulfanilamide degradation by peroxymonosulfate activation, *J. Hazard. Mater.*, 2022, **421**, 126794.
5. R. Li, X. Lu, B. Yan, N. Li, G. Chen, Z. Cheng, L. a. Hou, S. Wang and X. Duan, Sludge-derived biochar toward sustainable Peroxymonosulfate Activation: Regulation of active sites and synergistic production of reaction oxygen species, *Chem. Eng. J.*, 2022, **440**, 135897.
6. S. Qu, Y. Yuan, X. Yang, H. Xu, A. K. Mohamed, J. Zhang, C. Zhao, L. Liu, B. Wang, X. Wang, J. Rinklebe, Y. C. Li and S. Wang, Carbon defects in biochar facilitated nitrogen doping: The significant role of pyridinic nitrogen in peroxymonosulfate activation and ciprofloxacin degradation, *Chem. Eng. J.*, 2022, **441**, 135864.
7. Y. Zhang, M. Xu, R. He, J. Zhao, W. Kang and J. Lv, Effect of pyrolysis temperature on the activated permonosulfate degradation of antibiotics in nitrogen and sulfur-doping biochar: Key role of environmentally persistent free radicals, *Chemosphere*, 2022, **294**, 133737.
8. K. Xiao, F. Liang, J. Liang, W. Xu, Z. Liu, B. Chen, X. Jiang, X. Wu, J. Xu, J. Beiyuan and H. Wang, Magnetic bimetallic Fe, Ce-embedded N-enriched porous biochar for peroxymonosulfate activation in metronidazole degradation: Applications, mechanism insight and toxicity evaluation, *Chem. Eng. J.*, 2022, **433**, 134387.
9. R. Ma, X. Yan, X. Mi, Y. Wu, J. Qian, Q. Zhang and G.-H. Chen, Enhanced catalytic degradation of aqueous doxycycline (DOX) in Mg-Fe-LDH@biochar composite-activated peroxymonosulfate system: Performances, degradation pathways, mechanisms and environmental implications, *Chem. Eng. J.*, 2021, **425**, 131457.
10. Y. Lei, X. Guo, M. Jiang, W. Sun, H. He, Y. Chen, K. Thummavichai, O. Ola, Y. Zhu and N. Wang, Co-ZIF reinforced cow manure biochar (CMB) as an effective peroxymonosulfate activator for degradation of carbamazepine, *Applied Catalysis B: Environmental*, 2022, **319**, 121932.
11. W. Huang, Y. Tang, X. Zhang, J. Chen, Y. Lu, J. Luo and J. Zhang, Degradation of Sulfadiazine by Activated Peroxymonosulfate on Biochar with Different Carbon Structures, *International Journal of Environmental Research*, 2022, **17**, 13.
12. W. Zhang, L. Yan, Q. Wang, X. Li, Y. Guo, W. Song and Y. Li, Ball milling boosted the activation of peroxymonosulfate by biochar for tetracycline removal, *Journal of Environmental Chemical Engineering*, 2021, **9**, 106870.

13. S. Gao, J. Pan, Y. Zhang, Z. Zhao and J. Cui, Mn-NSC co-doped modified biochar/permonosulfate system for degradation of ciprofloxacin in wastewater, *Colloids and Surfaces A: Physicochemical and Engineering Aspects*, 2024, **680**, 132640.
14. W. Xu, F. Liang, Z. Liu, S. Li, J. Li, X. Jiang, S. C. Pillai, X. Wu and H. Wang, Rational design of animal-derived biochar composite for peroxymonosulfate activation: Understanding the mechanism of singlet oxygen-mediated degradation of sulfamethoxazole, *Environ. Pollut.*, 2024, **340**, 122807.
15. J. Li, J. Wei, M. Xu, G. Pan, Y. Zhang, L. Xing, Y. Li, J. Li and Z. Jiang, A porous graphitic biochar wrapped Co9S8 core–shell composite enables pH-universal activation of peroxymonosulfate for highly efficient and rapid antibiotics degradation, *Environmental Science: Nano*, 2022, **9**, 3629-3645.
16. N. T. Dung, V. D. Thao, N. P. Thao, C. T. M. Thuy, N. H. Nam, L. V. Ngan, K.-Y. A. Lin, T. C. Khiem and N. N. Huy, Turning peroxymonosulfate activation into singlet oxygen-dominated pathway for ofloxacin degradation by co-doping N and S into durian peel-derived biochar, *Chem. Eng. J.*, 2024, **483**, 149099.
17. F. Li, Z. Wan, D. Zheng, L. Zhang, W. Huang, F. Chen, J. Deng, Z. Qi, G. Li and F. Zhang, Self-dispersed Fe single-atom anchored biochar derived from hyperaccumulator residues with intrinsic Zn and Fe for selective peroxymonosulfate activation via electron transfer process, *Chem. Eng. J.*, 2024, **482**, 149052.
18. Y. Wang, Z. Liu, P. Huang, B. Lei, L. Qiao, T. Li, K.-Y. A. Lin and H. Wang, Mechanochemical synthesis of biochar encapsulated FeMn nanoparticles with strong metal–carbon interactions for efficient degradation of tetracycline via activating peroxymonosulfate, *Chem. Eng. J.*, 2024, **479**, 147525.
19. P. Wang, Y. Zhang, J. Zhu, J. Wei, J. Qi, T. Cao and M. Yang, Catalytic degradation of BPA by bamboo leaf-derived KOH-activated porous biocarbon loaded with CoFe2O4-activated peroxymonosulfate, *Chem. Eng. J.*, 2024, **492**, 151886.
20. L. Niu, Q. Lei, T. Zhao, Z. Tang, Y. Cai, D. Hou, S. Zhang, M. Fang, G. Hou, X. Zhao and F. Wu, In situ N-doping engineered biochar catalysts for oxidation degradation of sulfadiazine via nonradical pathways: Singlet oxygen and electron transfer, *Sci. Total Environ.*, 2024, **939**, 173206.
21. Y.-X. Huang, L.-Q. Yu, K.-Y. Chen, H. Wang, S.-Y. Zhao, B.-C. Huang and R.-C. Jin, Biochar with self-doped N to activate peroxymonosulfate for bisphenol-A degradation via electron transfer mechanism: The active edge graphitic N site, *Chin. Chem. Lett.*, 2024, **35**, 109437.
22. Z. Sun, J. Li, X. Wang, Y. Zhang and S. Xia, MgFe2O4/MgO modified biochar with oxygen vacancy and surface hydroxyl groups for enhanced peroxymonosulfate activation to remove sulfamethoxazole through singlet oxygen-dominated nonradical oxidation process, *Chem. Eng. J.*, 2023, **477**, 146960.
23. A. M. Aslandaş, N. Balcı, M. Arık, H. Şakiroğlu, Y. Onganer and K. Meral, Liquid nitrogen-assisted synthesis of fluorescent carbon dots from Blueberry and their performance in Fe3+ detection, *Appl. Surf. Sci.*, 2015, **356**, 747-752.
24. J. Guo, J. Xu, X. Liu, L. Dai, C. Zhang, X. Xiao and K. Huo, Enabling dual valorization of lignocellulose by fluorescent lignin carbon dots and biochar-supported persulfate activation: Towards waste-treats-pollutant, *J. Hazard. Mater.*, 2022, **435**, 129072.
25. W. B. Zhao, K. K. Liu, S. Y. Song, R. Zhou and C. X. Shan, Fluorescent Nano-Biomass Dots: Ultrasonic-Assisted Extraction and Their Application as Nanoprobe for Fe(3+)

detection, *Nanoscale research letters*, 2019, **14**, 130.
26. J. Yu, C. Xu, Z. Tian, Y. Lin and Z. Shi, Facilely synthesized N-doped carbon quantum dots with high fluorescent yield for sensing Fe3+, *New J. Chem.*, 2016, **40**, 2083-2088.
27. A. Ananthanarayanan, X. Wang, P. Routh, B. Sana, S. Lim, D.-H. Kim, K.-H. Lim, J. Li and P. Chen, Facile Synthesis of Graphene Quantum Dots from 3D Graphene and their Application for Fe3+ Sensing, *Adv. Funct. Mater.*, 2014, **24**, 3021-3026.
28. Y. Song, N. Qi, K. Li, D. Cheng, D. Wang and Y. Li, Green fluorescent nanomaterials for rapid detection of chromium and iron ions: wool keratin-based carbon quantum dots, *RSC Advances*, 2022, **12**, 8108-8118.